Nanoscale

Accepted Manuscript

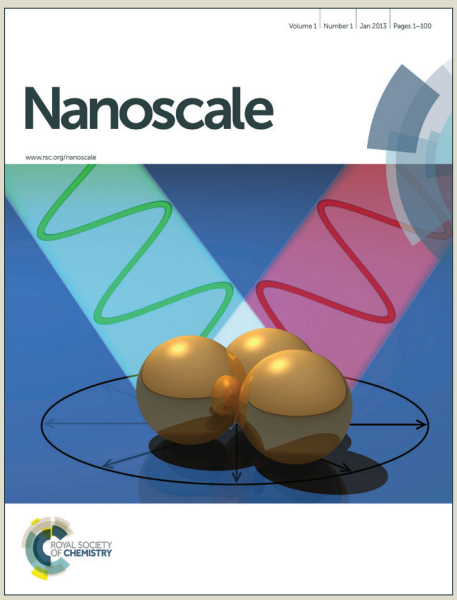

ROYAL SOCIETY OF CHEMISTRY

www.rsc.org/nanoscale

Nanoscale

RSCPublishing

ARTICLE

Journal Name ARTICLE

Cisplatin-tethered gold nanospheres for multimodal chemo-radiotherapy of Glioblastoma

Cite this: DOI: 10.1039/x0xx00000x

Received 00th January 2012,
Accepted 00th January 2012

DOI: 10.1039/x0xx00000x

www.rsc.org/nanoscale

*Sonali Setua,[a,b] Myriam Ouberai,[a] Sara G. Piccirillo,[b] Colin Watts[b] and Mark Welland[*a]*

Glioblastoma Multiforme (GBM) remains the most aggressive and challenging brain tumour to treat. We report first successful chemo-radiotherapy on patient derived treatment resistant GBM cells using a cisplatin-tethered gold nanosphere. After intracellular uptake, the nanosphere effects DNA damage which initiates caspase-mediated apoptosis in those cells. In the presence of radiation, both gold and platinum of cisplatin, serve as high atomic number radiosensitizers leading to the emission of ionizing photoelectrons and Auger electrons. This resulted in enhanced synergy between cisplatin and radiotherapy mediated cytotoxicity, and photo/Auger electron mediated radiosensitisation leading to complete ablation of the tumour cells in an *in vitro* model system. This study demonstrates the potential of designed nanoparticles to target aggressive cancers in the patient derived cell lines providing a platform to move towards treatment strategies.

1. Introduction

Nanotechnology has significant potential to revolutionize cancer diagnosis and therapy by developing engineered nanoparticles (NPs) that deliver targeted and controlled therapeutic actions.[1,2] The NPs can be functionalized with specific targeting ligands for efficient delivery of the therapeutics in the diseased tissue.[3] In addition, NPs can be loaded with imaging probes, which enable early diagnosis of the disease, surgical planning and *in vivo* monitoring of the treatment.[4] Over the past 20 years, various cancer-nanomedicine have been approved for clinical use.[5,6] Some of them have even become the standard of care for particular types of cancer.[7]

GBM is the most common and aggressive adult primary brain cancer[8] which is characterized by genetic instability and complex evolutionary dynamics. Histopathological diversity of GBM results in different clinical phenotypes, whose common feature is the rapid emergence of treatment resistance. There are several reasons for the poor prognosis of the GBM patients. First, although GBM rarely metastasizes outside the central nervous system, tumour cells diffusively invade surrounding healthy brain tissue.[9] This invasion

makes complete surgical excision of the tumour virtually impossible. Second, the selective permeability of the blood-brain barrier (BBB), together with the presence of efflux pumps, multidrug resistance proteins and degrading enzymes, decreases the bioavailability of the chemotherapeutics in diseased tissue.[10] Finally, the intrinsic radioresistance[11] and chemoresistance[12,13] of the GBM cells, which results from the genetic transformation and tumour heterogeneity, have made them refractory to conventional therapies. Recently, combination of temozolomide (TMZ, a DNA alkylating agent) + radiotherapy (RT) has improved the therapeutic outcome with limited survival benefit.[14] The median overall survival (OS) was 14.6 months for RT/TMZ compared to the OS of 12.1 months for RT alone. Moreover, epigenetic silencing of the DNA repairing gene is a prerequisite for the success of this approach[15] which, in turn, requires postoperative local chemotherapy of limited utility.[16] Overall, the shortcomings of current therapeutic strategies highlight the need for effective and generic multimodal therapeutic strategies.

Recently, the application of nanomedicine for GBM therapy has emerged as a promising alternative that can overcome the hurdles of the conventional therapies.[17] Among the various types of systems that have been used for GBM therapy, gold NPs (AuNPs) appeared to be the most appealing nanosystem because of their biocompatibility, small size, easy synthesis, tunable surface functionalities and enhanced CT and MRI contrast capabilities.[18,19] By using antibody tagged gold nanoshells, Bernardi *et al.* have reported targeted photothermal ablation of human glioma cells *in vitro*.[20] Using a different approach Baek *et al.* have used gold nanoshell loaded macrophages for delivery of these particles in the glioma spheroids followed by photo-thermal therapy of the glioma cells using near infrared (NIR) light.[21] However, the limited penetration depth of NIR restricts the clinical use of this strategy for human *in vivo* application.[22] Interestingly, using commercially available cell lines recent studies have reported that AuNPs can act as radiosensitizer in GBM treatment. The dose enhancing capacity of Au comes from its strong photoelectric absorption coefficient than the surrounding tissues, owing to the high atomic number (Z=79) of Au.[23] By using 11 nm sized AuNPs, Hainfeld *et al.* reported 50% long term (> 1 yr) tumour free survival of T-2449 GBM bearing mice as compared to the 9% survival rate of the control mice treated only with RT.[24] Joh *et al.* have demonstrated that in the presence of RT, PEG capped AuNPs can selectively accumulate in the U251 GBM tumours *in vivo* by BBB disruption that led to improved killing of the tumour cells.[25] In another study, Bobyk *et al.* have established *in vitro* and *vivo* radiosensitizing capacity of 15 nm AuNPs using F98 glioma cells.[26] However, unlike cells derived under serum free condition, these commercially available cell lines do not represent the actual malignancy of the patient disease[27,28] and thus questions the applicability of this approach in human GBM patient.

To address these challenges, we developed a multifunctional generic nanomedicine for combined chemo-radiotherapy of GBM. This strategy takes advantage of higher penetrating capacity of ionizing radiation compared to that of NIR, which is needed for brain cancer therapy in human patients. Critically, we used patient derived cell lines that were derived using serum free cell derivation technology, so that our therapeutic approach could be tested against evolving and drug resistant tumors.

At first, using PEI (Polyethylenimine, a positively charged polymer) capped AuNPs (AuNPs-PEI) we confirmed that even after highly improved intracellular (nuclear and cytosolic) delivery AuNPs alone cannot radiosensitise patient derived GBM cells adequately.

Thereafter, we developed a multifunctional nanosphere that comprises AuNPs surface engineered with the anticancer drug cisplatin (AuNPs-Pt) (Fig. 1). The nanosphere demonstrated

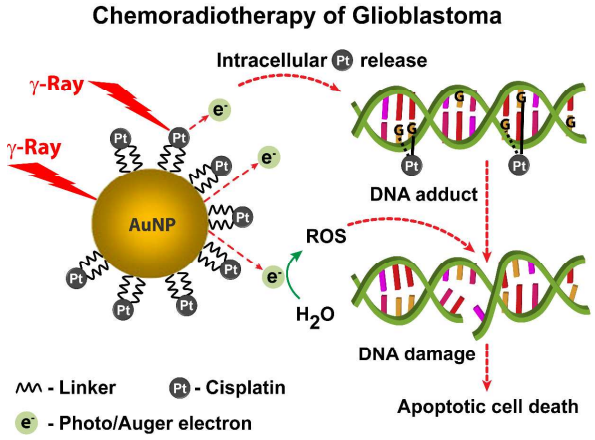

Fig.1 Multifunctional nanosphere for combined chemo-radiotherapy. Principle of nanosphere action based on gold and platinum mediated radiosensitization and cisplatin induced genotoxic damage.

intracellular (cytosolic) uptake into live patient-derived cell lines. Once established within the cancer cells, the nanosphere exhibited cisplatin mediated DNA damage eventually inducing cellular apoptosis. The combination of RT further augmented this damage.

Moreover, in the presence of RT, the gold, from the nanoparticle itself, and the platinum, from the cisplatin, preferentially absorbed radiation due to their strong photoelectric absorption coefficient resulting in the emission of photoelectrons and Auger electrons.[23,29] These high energy electrons hydrolyzed intracellular water leading to the production of cytotoxic reactive oxygen species (ROS).[30] The significant increase in the cytotoxicity, as a consequence of this combined therapeutic approach, led to efficient demolition of the tumour cells in an *in vitro* model system.

2. Experimental section

2.1 Cell culture

GBM cell lines (S1, S2 and SP56) were derived from the patient tumour sample as previously described.[27] In brief, tissue samples were obtained in accordance with local ethical guidelines. Anonymised tissue was minced in modified PBS before enzymatic digestion by accutase (Sigma, UK). Then, single cells were isolated by filtration through a 40 µm filter (Falcon, UK) and washed with 10 ml red blood cell lysis buffer (Roche, UK). Live cells were quantified by trypan blue (Sigma, UK) exclusion method, seeded at standard density of 15 x 10^3 cells/cm^2 in defined media and allowed to form primary aggregates. These were collected and plated, without dissociation, onto extracellular matrix (ECM) coated flasks (ECM 1:10 dilution, Sigma, UK) and allowed to form a primary monolayer. As the primary monolayer approached confluence, cells were dissociated using accutase at room temperature and washed with PBS. Cell viability was assessed by trypan blue and cells were reseeded onto ECM coated flasks at a density of 150 cells/cm^2 to generate the secondary monolayer. To generate subsequent monolayers cells were seeded at standard density 15,000 cells/cm^2 at each passage.

Cells were cultured in 10 ml serum free medium (phenol red-free Neurobasal A, Invitrogen, UK) with 20mM L-glutamine (Sigma, UK), 1% (v/v) penicillin/streptomycin/amphotericin B mix (Sigma, UK), 20 ng/ml hEGF (Sigma, UK), 20 ng/ml hFGF (R&D systems, UK), 2% (v/v) B27 (Invitrogen, UK) and 1% N2 (Invitrogen, UK) and incubated at 37 ºC in 5% CO2.

2.2 Synthesis and characterization of the nanoconjugates

Synthesis of AuNPs-PEI

AuNPs-PEI were synthesized by capping AuNPs (50 nm, BBI Solutions, UK) with HSA (Human serum albumin; Sigma, UK) and PEI (Polyethylenimine; Sigma, UK) using a layer-by-layer technique. 1ml of AuNP solution was incubated with 100 µl of HSA aqueous solution (0.2 µg/ml, pH 5) while stirring. After 30 mins, 60 µl of 0.01 wt% PEI (in 10 mM sodium phosphate buffer, pH 7.4) was added to the reaction mixture and incubated for another 30 mins at room temperature.

Synthesis of AuNPs-Pt

AuNPs-Pt were synthesized following the fundamental principle of a published protocol with further modifications.[31] 5 ml of AuNP solutions was mixed with 5 ml of 20 mM MUA (Mercaptoundecanoic acid; Sigma, UK) in ethanol and incubated at room temperature for overnight. MUA capped AuNPs were purified using zeba desalting column (MWCO 40K, Pierce, UK) as per manufacturer protocol. Purified AuNPs-MUA were reacted with 2 mg/ml aqueous cisplatin (Pt) (Sigma, UK) in the tricine buffer (Sigma, UK) at pH 8.3 for 1 h at room temperature. The resulting AuNPs-Pt were purified using zeba desalting column.

Characterization of the nanoconjugates

Scanning electron microscopy (SEM)

The size of the nanoconjugates were determined using LEO GEMINI 1530VP FEG-SEM (Carl Zeiss, Germany). SEM samples were prepared by drying 10 µl of the each formulation of the nanoconjugates on a silicon substrate.

Zeta potential measurement

The surface charge of the nanoconjugates were determined using Zetasizer Nano ZS (Malvern Instruments Ltd, UK) in ultrapure deionized (DI) water (pH 6).

Analysis of colloidal stability in physiological media

The physiological stability of the nanoconjugates in cell culture media (pH 7.4) were determined by using UltraSpec 2100 Pro

UV/Visible spectrophotometer (Aktiengesellschaft Corp. Ludwigshafen, Germany). Nanoconjugates were incubated in media for 24 hrs before analysis.

X-ray photoelectron spectroscopy

The elemental composition of the nanoconjugates was characterized by XPS analysis using K-Alpha XPS spectrometer (Thermo, UK).

2.3 Cell uptake studies

S2 cells were seeded on 13 mm ECM coated glass coverslips placed inside 24-well tissue-culture plate at seeding density of 6 x10^3 cells/cover glass and incubated overnight. Cells were treated with 0.087 mM of the different nanoconjugates. After PBS wash, cells were fixed with 4% Paraformaldehyde, blocked with 10% goat serum made in 0.1% Triton X -100 in PBS and stained with mouse monoclonal anti-nestin antibody (1:200, Millipore) overnight at 4ºC. Thrice washed cells were stained with Alexa-488 conjugated secondary antibody (1:500, Invitrogen) for 2 h at room temperature. The nucleus was counterstained with DAPI (Sigma). Cellular localization of the nanoconjugates was viewed using dark-field confocal microscopy (Leica BMI 6000B) and quantified using Imaris 7.4.2 software. Images were processed using ImageJ software.

2.4 MTS cell viability assay

MTS assay was performed to analyze the inherent toxicity of AuNPs-PEI. For MTS assay, CellTiter 96 Aqueous One Solution Cell Proliferation Assay kit (Promega, UK) was used. S2 cells were seeded at a density of 3×10^3 cells/well in 96-well tissue culture plate (Nunc, UK) pre-coated with ECM in 200µl of media and incubated overnight. The medium was replaced by fresh medium containing different concentrations (0.029, 0.058, 0.087, 0.116 and 0.145 mM) of AuNP-HSA/ AuNP-PEI. After 6 hrs, the medium was removed, the cells were washed twice with HBSS, and fresh medium was added. After another 2 days, 5µl of MTS solution was added in each well. After 4 hrs, incubation at 37°C with 5% CO2, optical absorbance values at 490 nm from each well were measured using a plate reader (ELx 800, Bio-Tek, UK). From the absorbance value percentage of the viable cells was calculated using the following equation:

% viability = (absorbance value of the cell treated with AuNPs-HSA/AuNPs-PEI / Absorbance value of the cells without treatment) x 100

2.5 Differential interference contrast (DIC) microscopy

The effect of AuNPs-PEI treatment on S2 cell morphology, which represents the cytotoxicity of the nanoconjugates, was imaged using DIC microscope (Nikon, U.S.A.).

2.6 γH2AX and Caspase assay

GBM cells were treated with nanoconjugates as before, washed with HBSS and irradiated using cesium-137 (Cs-137) beam radiator (Gamma services) at 1 Gy/minute. Cells were fixed and blocked as before and incubated with mouse monoclonal anti-γ-H2AX antibody (1:1000, Millipore) or rabbit polyclonal anti-cleaved caspase-3 antibody (1:100, Cell signalling) overnight at 4ºC. Thrice washed cells were stained with Alexa-488 (γH2AX) and Alexa-568 (caspase) conjugated secondary antibody (1:500, Invitrogen) for 2 h at room temperature. The nucleus was counterstained with DAPI. Image analysis was performed with Imaris 7.4.2 (γH2AX) and ImageJ (caspase) software.

2.7 Growth curve analysis

GBM cells were seeded at a density of 750×10^3 cells/T75 tissue culture flask pre-coated with ECM and incubated overnight. The medium was replaced by fresh medium containing 0.087 mM of the different nanoconjugates. After specific incubation time, the medium containing nanoconjugates was removed. Cells were washed with HBSS and irradiated using cesium-137 (Cs-137) beam radiator (Gamma service, UK) at 1 Gy/minute. Viable cells were counted using trypan blue exclusion method. At each time point, total number of viable cells (estimated total cell number) was calculated using the following equation :

Estimated total cell number = Total number of viable cell at the present time point x (Estimated total cell number at the previous time point / Number of the cells seeded at the previous time point).

3. Results and discussion

3.1 AuNPs-PEI in combination with RT failed to decrease the growth of GBM cells efficiently

The use of AuNPs as a novel radiosensitizer for cancer treatment has gathered momentum in recent times.[23] This dose enhancing ability of AuNPs has also been explored for GBM treatment using commercially available cell lines.[24,25,26] However, serum-free cell-derivation technology generates cells that more accurately represent patient disease.[27,28] Therefore, we first analyzed the radiosensitizing capacity of AuNPs in three patient-derived GBM cell lines, namely S1, S2 and SP56, which represent the heterogeneous, clonally variegated chemo-radio resistant cell populations found in patients.[32] For this purpose, we have used PEI capped AuNPs (AuNPs-PEI). PEI is a positively charged polymer that functions as a delivery vehicle in gene therapy.[33] PEI significantly improves intracellular delivery of large therapeutic cargo which even can enter in the nucleus of the cells[34] and thus increases the possibility of cytotoxic specially genotoxic damage. In the present study, using PEI as the capping agent, we tried to maximize the nuclear and cytosolic import of AuNPs in the patient derived GBM cells. According to the recent reports, this high amount of intracellular AuNPs, in combination with RT, were expected to maximize the cellular damage.[35,36]

Synthesis and characterization of AuNPs-PEI

AuNPs-PEI were synthesized by stabilizing AuNPs with HSA followed by surface capping with PEI (Fig. S1a). The resulting conjugate AuNP-PEI had a positive surface charge of 36 mV (Fig. S1b). SEM showed the presence of spherical nanoconjugate of an average diameter 51 nm (Fig. S1c). XPS confirmed the presence of Au in AuNPs-PEI that retains the characteristic photoelectron and Auger electron emission capacity even after surface functionalization (Fig. S1d and e). UV-Visible spectroscopy demonstrated that AuNPs-HSA and AuNPs-PEI can maintain their colloidal stability under the physiological pH (7.4) and high ionic strength of the cell culture media as indicated by their characteristic SPR (surface plasmon resonance) peak position at 530 nm corresponding to 50 nm sized AuNPs (Fig. S2a). This result guarantees their ability for efficient cell interaction[37] required for optimal cell uptake in an *in vitro* setting.

Cell uptake of AuNPs-PEI

The *in vitro* cell uptake of the nanoconjugates were analysed by dark-field confocal scanning microscopy. The result showed that AuNPs-PEI were internalized into S2 cells after 6 hrs of incubation (Fig. 2a, b). These internalized particles formed clusters in the cytoplasm as well as in the nucleus that was detected using the light scattering property of the AuNPs. Compared with the AuNPs-HSA, we observed 5 fold enhancements in the uptake of AuNPs-PEI (Fig. 2a, c). The positive surface charge of AuNPs-PEI helped them to interact with the negatively charged cell surface proteoglycans leading to the enhanced cell uptake.[38] Notably, the nuclear import of AuNPs-PEI (of size 51 nm which is much higher than the nuclear pore cut off i.e. < 10 nm) resulted from the nuclear membrane disruption by PEI.[39] Therefore, the highest concentration of AuNPs-PEI used for *in vitro* assays was limited to 0.087 mM (considering molar concentration of Au). Beyond this concentration, AuNPs-PEI decreased the viability of GBM cells (Fig. S3a) and destroyed their morphology (Fig. S3b) significantly.

Radiosensitizing potential of AuNPs-PEI

As a result of the improved cell uptake of AuNPs, compared to the cells receiving RT or AuNP-HSA + RT, AuNP-PEI + RT treated cells displayed an increased density of γH2AX foci indicating increased DNA double strand breaks (Fig. 2a, d, e). This enhanced DNA damage led to enhanced apoptotic activity indicated by increased activation of caspase-3 (Fig. 3a, b, c). Growth-curve analysis showed a reduced growth rate for the AuNP-PEI + RT group compared to the RT or AuNP-HSA + RT group (Fig. 3a, d). However, at day 25 post radiation, treatment-resistant cell populations emerged from RT, AuNP-HSA + RT and AuNP-PEI + RT groups. We observed a similar effect for another GBM cell SP56 (Fig. S4a, c), whereas AuNP-PEI + RT stopped the growth rate of the GBM cell S1 (Fig. S4a, b). These results suggest that, although GBM cells of different patients vary in the inherent radioresistance, AuNP + RT mediated monotherapy alone is unlikely to be effective for all patients.

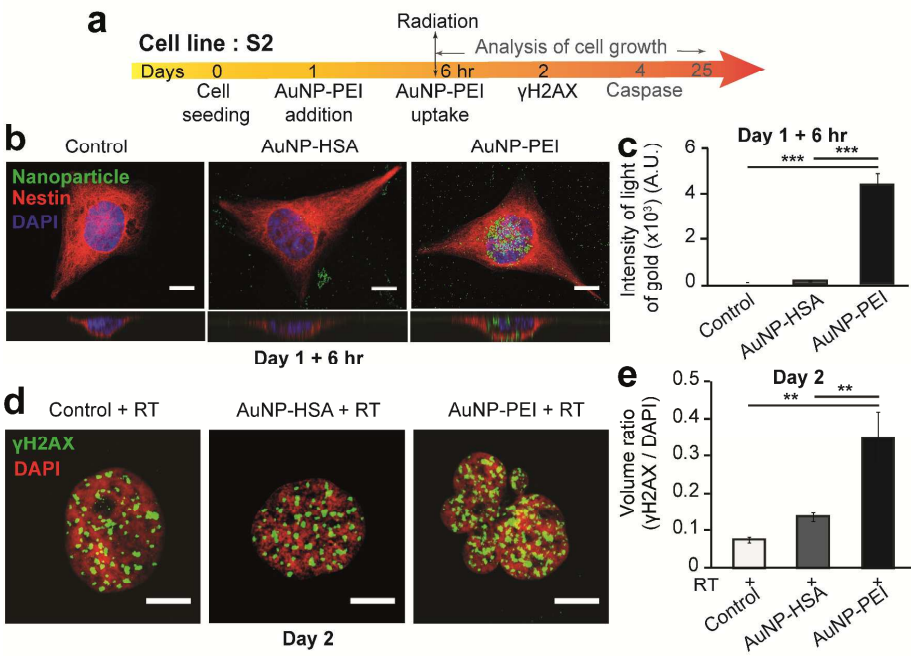

Fig. 2 *In vitro* cell uptake and cytotoxicity of AuNPs-PEI with radiation. a, Schematic diagram of the experimental design. b, Confocal images of S2 showing internalized AuNPs-PEI in the nucleus and cytoplasm of the cells. c, Quantitative analysis of scattered light's intensity of AuNPs-PEI. d,e, Representative images (d) and quantitative analysis (e) of γ-H2AX foci indicating DNA damage. RT= 10 Gy. Scale bars = 20 μm. Means ± s.e.m. (n=3). ** P<0.01; *** P < 0.001, ANOVA.

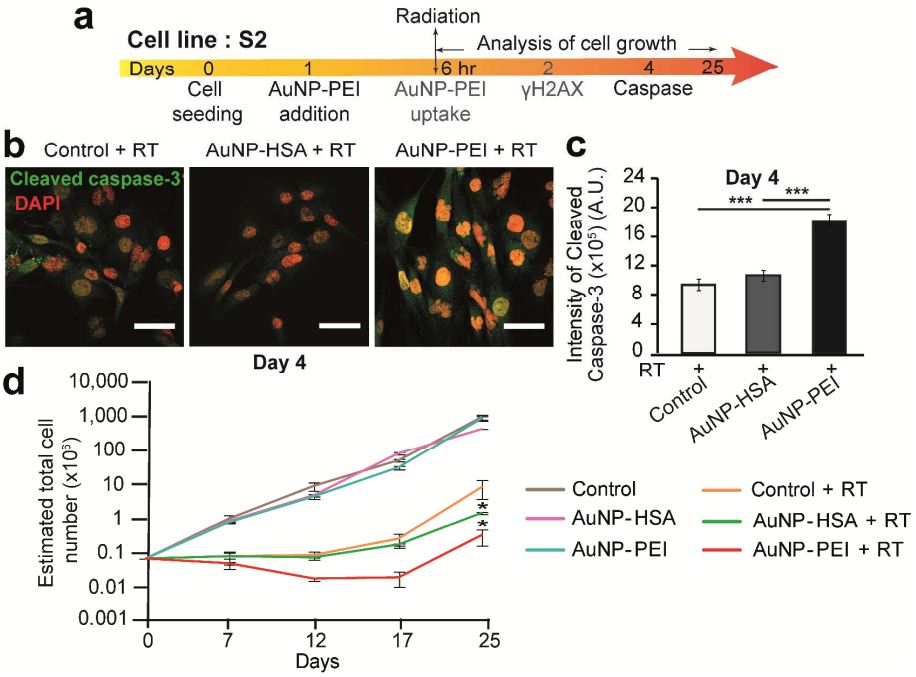

Fig. 3 Effect of AuNPs-PEI mediated radiosensitization on S2 cells. a, Schematic diagram of the experimental design. b, c, Representative images (b) and quantitative analysis (c) of cleaved caspase-3 indicating apoptosis. d, Patterns of *in vitro* cell growth of different treatment groups of S2 cells. RT= 10 Gy. Scale bars = 20 μm. Means ± s.e.m. (n=3). * P<0.05; *** P < 0.001, ANOVA.

3.2 AuNPs-Pt mediated combined chemoradiotherapy can abrogate treatment resistance in GBM therapy

To overcome the limiting therapeutic ability of AuNPs, as discussed above, we devised the multifunctional nanosphere comprising AuNPs surface functionalized with anticancer drug cisplatin (AuNPs-Pt). Cisplatin is the most common metallodrug used for the treatment of a variety of solid tumours.[40] The cytotoxicity of cisplatin results mainly from the formation of bifunctional DNA cross-links by interacting with N^7 atom of purine bases in DNA.[41] These cross-links inhibit DNA replication, which ultimately trigger apoptosis.[42]

Synthesis and characterization of AuNPs-Pt

To fabricate AuNPs-Pt, MUA was first adhered to the AuNP surface via thiol anchor group. Subsequently, the aqua (H_2O^+) group of aquated cisplatin molecules were bound to the COOH group of MUA through a pH sensitive coordination bond (Fig. 4a). This strategy ensures that the bond between MUA and cisplatin will remain stable under physiological pH (7.2 to 7.6) and only at acidic pH of 4.4, which corresponds to the late endosomal pH cisplatin will be released from the AuNPs.[31] Moreover, in this configuration, the inert NH_3 moieties of cisplatin are exposed to the exterior whereas the reactive aqua (H_2O^+) group remains conserved for interaction with DNA. Therefore, this approach can also protect the drug against plasma deactivation *in vivo*.[43,44] After MUA capping the average surface charge of the of the AuNPs shifted from - 40 mV to - 44 mV. After reacting with cisplatin, the surface charge of the final conjugate (AuNP-Pt) further shifted to - 30 mV that resulted from the quenching of the negative surface charge of MUA by cisplatin molecules attached with it[31] (Fig. 4b). UV-Vis absorption spectroscopy proved that both AuNPs-MUA and AuNPs-Pt can retain their colloidal stability, under the physiological pH (7.4) and high ionic strength of the cell culture media (Fig. S2b). The colloidal stability of the nanoconjugates in physiological media is a prerequisite for their optimal cell uptake[37] and therapeutic efficacy. SEM showed the presence of spherical nanosphere of average diameter 50 nm (Fig. 4c). XPS confirmed the presence of gold and platinum in AuNPs-Pt that retains the characteristic photoelectron and Auger electron emission capacity even after surface functionalization (Fig. 4d, e). The average number of cisplatin (approximately 1.7 x 10^4) and MUA (approximately 4 x 10^4) on one AuNP was calculated by measuring the gold-to-platinum, and gold-to-sulphur atom ratio acquired with XPS (Fig. 4f).

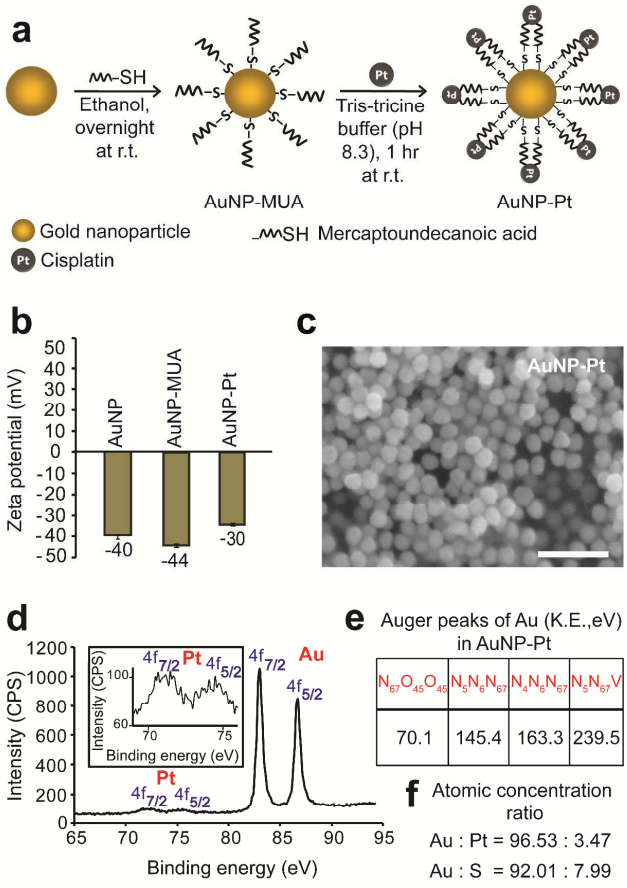

Fig. 4 Synthesis and characterization of AuNPs-Pt. a, Schematic showing preparation of AuNPs-Pt. b, Zeta potential of AuNPs, AuNPs-MUA and AuNPs-Pt, Means ± stdev (n=3). c, SEM image of AuNPs-Pt (scale bar = 0.2 µm). d, e, XPS analysis of AuNPs-Pt showing the presence of gold and platinum as demonstrated by the photoelectron peaks of gold and platinum (d) and Auger peak positions of gold (e). f, Atomic concentration ratio of gold:platinum and gold:sulphur, present in AuNP-Pt, as observed by XPS analysis.

In vitro cell uptake and therapeutic potential of AuNPs-Pt

At first, we analyzed the chemotherapeutic effect of AuNPs-Pt in treatment resistant S2 cells using similar concentration (0.087 mM) of nanoconjugates as used in case of AuNPs-PEI. Cells treated with AuNPs-MUA serves as control showing therapeutic ability of AuNPs alone. Although, after 1 day of incubation with cells (day 2),

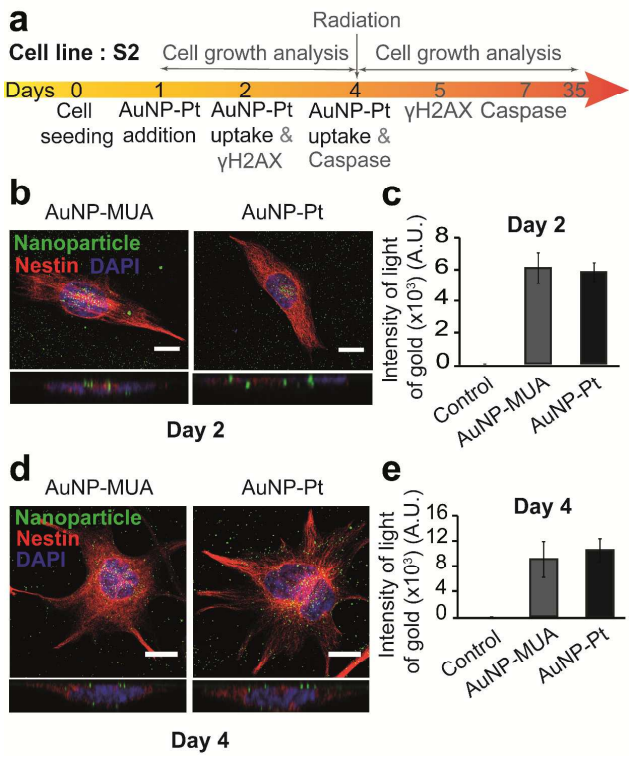

Fig. 5 *In vitro* cell uptake of AuNPs-Pt. a, Schematic diagram of the experimental design. b, d, Confocal images of S2 showing internalized AuNP-MUA and AuNPs-Pt at day 2 (b) and day 4 (d) in the cytoplasm and perinuclear region of the cells. c, e, Quantitative analysis of scattered light's intensity of internalized AuNPs-MUA and AuNPs-Pt at day 2 (c) and day 4 (e). Scale bars = 20 µm. Means ± s.e.m. (n=3). Statistical analysis was performed by ANOVA.

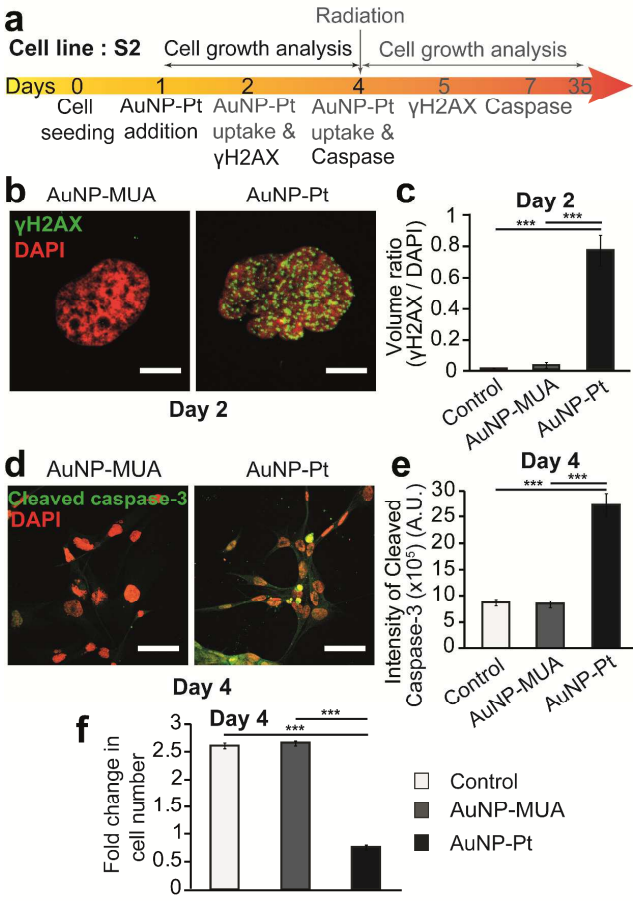

Fig. 6 Chemotherapeutic potency of AuNPs-Pt. a, Schematic diagram of the experimental design. b, c, Representative images (b) and quantitative analysis (c) of γ-H2AX foci indicating DNA damage. d, e, Representative image (d) and quantitative analysis (e) of cleaved caspase-3 indicating apoptosis. f, Fold change in cell number of different treatment groups at day 4 compared to day 0. Scale bars = 20 µm. Means ± s.e.m. (n=3). *** $P < 0.001$, ANOVA.

the extent of uptake of AuNP-MUA and AuNP-Pt was comparable (Fig. 5a, b, c) we observed activation of γH2AX foci only in the AuNP-Pt treated cells (Fig. 6a, b, c). This observation indicates that the nanosphere could deliver sufficient amount of cisplatin into the cell through endocytosis.[45] At the acidic pH of the late endosome the bond between cisplatin and AuNPs was broken.[31] The active and free cisplatin molecules (M.W 300D, which corresponds to < 1 nm size) diffused out of the endosomal compartment, passed through the nuclear pore and reached the DNA resulting in DNA damage.[41] At day 4, we observed further increase in the cellular internalization of the AuNP-MUA and AuNP-Pt (Fig. 5a, d, e). Eventually, AuNP-Pt treatment led to the activation of caspase-3 (Fig. 6a, d, e), which decreased cell growth rate significantly, unlike AuNP-MUA treated cells (Fig. 6f).

In the next step, we evaluated the synergistic chemo-radiotherapeutic potential of this nanosphere using S2 cells. After irradiation at day 4, compared to the RT or AuNP-MUA + RT, the AuNP-Pt + RT group showed significant enhancement in the DNA double strand break as indicated by the increased density of γH2AX foci (Fig. 7a, b, c). This increased DNA damage led to enhanced activation of caspase-3, resulting in significant improvement in the rate of apoptosis (Fig. 7a, d, e). Growth curve analysis (Fig. 7f) showed that, until day 20, RT and AuNP-MUA + RT caused similar decreases in the cell growth rate. Beyond this time-point, the AuNP-MUA + RT showed emergence of treatment-resistant clones, which gradually increased till day 35. However, this combination could not

stop the growth of these malignant cells, which indicates the risk of recovery with time. From the beginning, AuNP-Pt + RT showed significant improvement in growth arrest, which was comparable to the AuNP-Pt group. However, after day 16, the cells in the latter group started to recover from damage and ultimately acquired the growth rate of RT group by day 35. In contrast, the damage imparted by AuNP-Pt + RT was so significant that the growth rate of this group continued to decrease, which eventually led to the complete ablation of the tumour cells. A similar effect was observed in the growth curve analysis of two additional patient-derived cell lines, S1 and SP56 (Fig. S5a, b, c). Together, these results reveal that, AuNPs-Pt mediated multimodal chemo-radiotherapy has the potential to abrogate treatment resistance in GBM cells effectively.

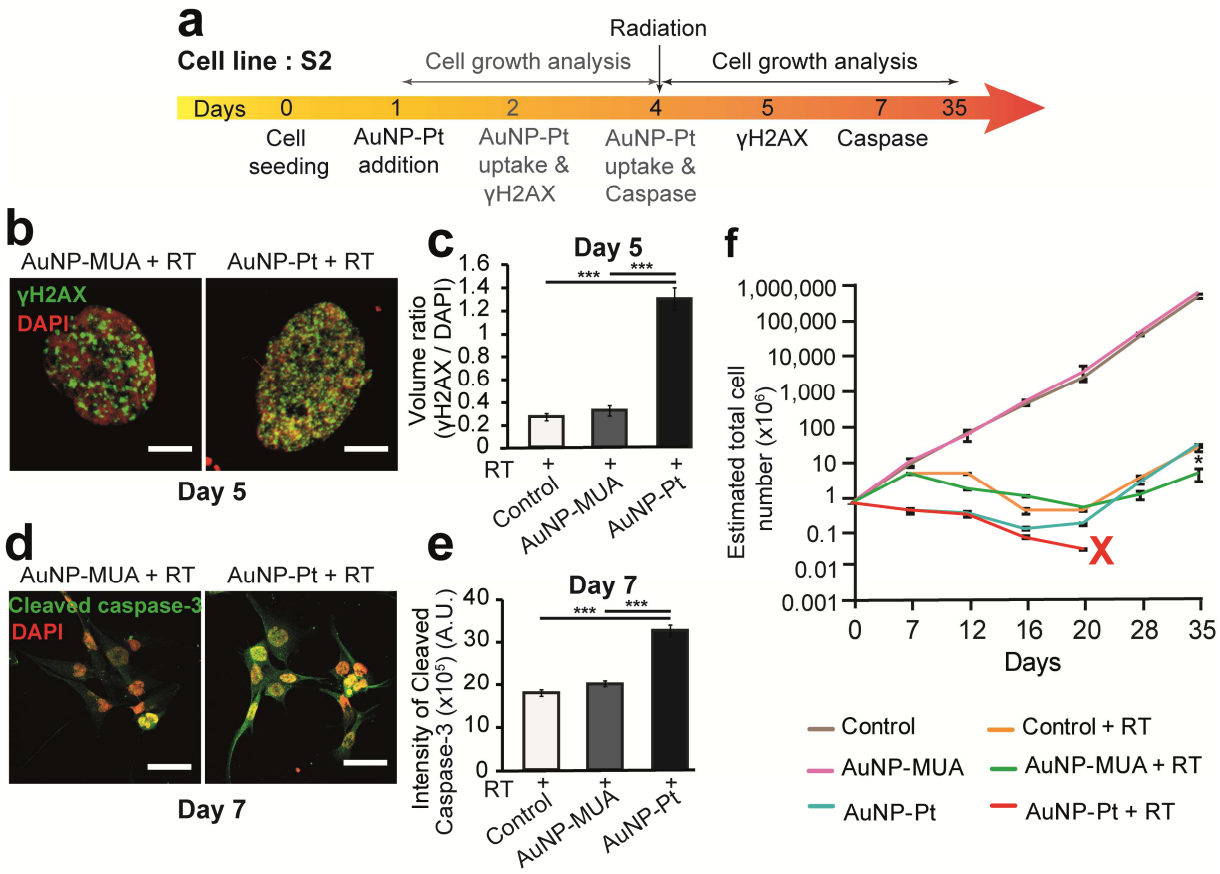

Fig. 7 Effect of AuNPs-Pt mediated chemo-radiotherapy on S2 cells. a, Schematic diagram of the experimental design. b, c, Representative images (b) and quantitative analysis (c) of γ-H2AX foci indicating DNA damage. d, e, Representative images (d) and quantitative analysis (e) of cleaved caspase-3 indicating apoptosis. Scale bars = 20 μm. Means ± s.e.m. (n=3). *** $P < 0.001$, ANOVA. f, Patterns of *in vitro* cell growth of different treatment groups. Means ± s.e.m. (n=3). *$P < 0.05$, Student's t-test. RT= 10 Gy.

It should be pointed out that, in case of AuNPs-MUA and AuNPs-Pt treated cells the AuNPs were confined in the cytosolic vesicles and thus were unable to enter in the nucleus (Fig. 5a, b, d). In contrast, PEI capped AuNPs could reach both cytosol as well as the nucleus of the cells (Fig. 2a, b) thereby enhancing the probability of AuNPs + RT mediated lethal genotoxic damage.[35] However, in the presence of RT, AuNPs-PEI failed to radiosensitise patient GBM cells adequately (Fig. 3d). The long term therapeutic effect of AuNPs-PEI on GBM growth rate is comparable to that of AuNPs-MUA (Fig. 7f). Eventually in both cases a re-growth of treatment resistant GBM cells was observed in contrast to the cells that received AuNPs-Pt + RT treatment. This finding further strengthens our conclusions that unlike AuNPs + RT, AuNPs-Pt in combination with RT can act as a potential therapeutic modality for GBM

treatment.

This proof-of-concept study showed promises that AuNPs-Pt mediated multimodal treatment can overcome the challenges of current GBM therapies. However, before transferring this technology for human clinical trials particular issues need to be considered carefully. First, to prove the chemo-radiotherapeutic potential of AuNPs-Pt using *in vitro* model system, we have used Cs-137 as the irradiation source which is used in brachytherapy. The energy of Cs-137 i.e. 662 KeV is enough to produce ionizing photoelectrons and Auger electrons from AuNPs as the K edge of Au is 80 KeV.[46] Similar to this study, several groups have used Cs-137 as a radiation source and successfully demonstrated the radiosensitizing capacity of gold nanoparticles in various cancers.[19,47,48] However, in clinical setting ionizing radiation of MeV energy is better suited than KeV energy as it does not suffer the strong tissue attenuation problem observed in the latter.[23] On the contrary, the probability of photoelectrons and Auger electrons production through photoelectric effect is lesser at MeV energy range compared to KeV energy.[49] Therefore, for clinical application of this technology use of new generation Linacs (Linear accelerator, source of MeV energy), which are flattening filter free and thus can increase the radiation dose deposition rate, would be necessary. Second, to ensure optimal cell uptake of the nanosphere, which is a prerequisite to achieve maximum efficacy of any therapeutics, we selected 50 nm sized AuNPs.[50] However, for *in vivo* application of this technology, the size of the nanomedicine should be restricted to ~ 6 nm that is the upper limit of safe renal clearance.[51] This modification will require the use of smaller sized AuNPs with proper surface chemistry that can overcome toxicity concern related to long-term accumulation NPs in the body.[52,31] In this context, the recent findings of Miladi *et al.* demonstrating radiosensitizing potential of ultrasmall Au@DTDTPA suitable for renal clearance holds significant importance.[52,19] This ultrasmall nanosystem was also tractable by high resolution MRI, which helped to optimize RT schedule *in vivo*. Therefore, it will be rational to develop cisplatin conjugated magnetic core-gold shell nanosphere that can be visualized by MRI and will have a appropriate size and surface chemistry for optimal biodistribution and renal clearance.

4. Conclusion

In summary, we report the proof-of-concept for the strategy to develop a generic nanomedicine suitable for multimodal therapeutic targeting of challenging cancers such as GBM. Using patient derived treatment resistant cells, we have established that AuNP-Pt-mediated concomitant chemo-radiotherapy is a potential therapeutic modality that can overcome the limitations of standard treatment. Vehiculation of cisplatin using AuNP will modify the pharmacokinetics of this drug resulting in a significant decrease in cisplatin-induced systemic toxicity.[31] By combining this new approach with cancer cell-targeting probes, a tumour targeted 'theranostics' can be developed in the future.[53] This will provide a more tractable, specific and efficient therapeutic strategy for treatment of GBM and other challenging cancers.

Acknowledgements

This work was supported by a Cambridge Commonwealth, European and International Trust's research fellowship (S.S.), the Biotechnology and Biological Sciences Research Council (BBRSC) Grant (BB/H003843/1) (M.O.), Marie Curie Intra-European Fellowship from the European Commission Seventh Framework Programme (S.G.P.). S.S. is thankful to Dr. Swadhin Chandra Jana, IGC, Portugal for help in image analysis. Authors thank Dr. Jose Portoles and Prof. Peter Cumpson, Nexus Nanolab, Newcastle University for XPS analysis.

Notes

[a] Nanoscience Centre, Department of Engineering, University of Cambridge, Cambridge CB3 0FF, United Kingdom.
[b] John van Geest Centre for Brain Repair, Department of Clinical Neurosciences, University of Cambridge, Forvie Site, Robinson Way, Cambridge CB2 0PY, United Kingdom.

Electronic Supplementary Information (ESI) available: Additional figures. See DOI: 10.1039/b000000x/

References

1. S. Akhter, I. Ahmad, M. Z. Ahmad, F. Ramazani, A. Singh, Z. Rahman, F. J. Ahmad, G. Storm and R. J. Kok, *Curr. Cancer Drug Targets*, 2013, **13**, 362-378.
2. J. D. Meyers, T. Doane, C. Burda and J. P. Basilion, *Nanomedicine (Lond)*, 2013, **8**, 123-143.
3. M. J. Akhtar, M. Ahamed, H. A. Alhadlaq, S. A. Alrokayan and S. Kumar, *Clin. Chim. Acta*, 2014, **436C**, 78-92.
4. F. M. Kievit and M. Zhang, *Adv. Mater.*, 2011, **23**, H217-247.
5. D. Peer, J. M. Karp, S. Hong, O. C. Farokhzad, R. Margalit and R. Langer, *Nat. Nanotechnol.*, 2007, **2**, 751-760.
6. M. E. Davis, Z. G. Chen and D. M. Shin, *Nat. Rev. Drug Discov.*, 2008, **7**, 771-782.
7. W. J. Gradishar, S. Tjulandin, N. Davidson, H. Shaw, N. Desai, P. Bhar, M. Hawkins and J. O'Shaughnessy, *J. Clin. Oncol.*, 2005, **23**, 7794-7803.
8. A. Behin, K. Hoang-Xuan, A. F. Carpentier and J. Y. Delattre, *Lancet*, 2003, **361**, 323-331.
9. C. B. Wilson, *Clin. Neurosurg.*, 1992, **38**, 32-48.
10. Y. Chen and L. Liu, *Adv. Drug Deliv. Rev.*, 2012, **64**, 640-665.
11. S. Bao, Q. Wu, R. E. McLendon, Y. Hao, Q. Shi, A. B. Hjelmeland, M. W. Dewhirst, D. D. Bigner and J. N. Rich, *Nature*, 2006, **444**, 756-760.
12. J. Chen, Y. Li, T. S. Yu, R. M. McKay, D. K. Burns, S. G. Kernie and L. F. Parada, *Nature*, 2012, **488**, 522-526.
13. D. Beier, J. B. Schulz and C. P. Beier, *Mol. Cancer*, 2011, **10**, 128.
14. R. Stupp, W. P. Mason, M. J. van den Bent, M. Weller, B. Fisher, M. J. Taphoorn, K. Belanger, A. A. Brandes, C. Marosi, U. Bogdahn, J. Curschmann, R. C. Janzer, S. K. Ludwin, T. Gorlia, A. Allgeier, D. Lacombe, J. G. Cairncross, E. Eisenhauer and R. O. Mirimanoff, *N. Engl. J. Med.*, 2005, **352**, 987-996.
15. M. E. Hegi, A. C. Diserens, T. Gorlia, M. F. Hamou, N. de Tribolet, M. Weller, J. M. Kros, J. A. Hainfellner, W. Mason, L. Mariani, J. E. Bromberg, P. Hau, R. O. Mirimanoff, J. G. Cairncross, R. C. Janzer and R. Stupp, *N. Engl. J. Med.*, 2005, **352**, 997-1003.
16. S. Nagpal, *Neurosurg. Clin. N. Am.*, 2012, **23**, 289-295, ix.
17. E. K. Nduom, A. Bouras, M. Kaluzova and C. G. Hadjipanayis, *Neurosurg. Clin. N. Am.*, 2012, **23**, 439-449.
18. A. J. Mieszawska, W. J. Mulder, Z. A. Fayad and D. P. Cormode, *Mol. Pharm.*, 2013, **10**, 831-847.
19. I. Miladi, C. Alric, S. Dufort, P. Mowat, A. Dutour, C. Mandon, G. Laurent, E. Brauer-Krisch, N. Herath, J. L. Coll, M. Dutreix, F. Lux, R. Bazzi, C. Billotey, M. Janier, P. Perriat, G. Le Duc, S. Roux and O. Tillement, *Small*, 2014, **10**, 1116-1124.
20. R. J. Bernardi, A. R. Lowery, P. A. Thompson, S. M. Blaney and J. L. West, *J. Neurooncol.*, 2008, **86**, 165-172.
21. S. K. Baek, A. R. Makkouk, T. Krasieva, C. H. Sun, S. J. Madsen and H. Hirschberg, *J. Neurooncol.*, 2011, **104**, 439-448.
22. X. Gao, Y. Cui, R. M. Levenson, L. W. Chung and S. Nie, *Nat. Biotechnol.*, 2004, **22**, 969-976.
23. K. T. Butterworth, S. J. McMahon, F. J. Currell and K. M. Prise, *Nanoscale*, 2012, **4**, 4830-4838.
24. J. F. Hainfeld, H. M. Smilowitz, M. J. O'Connor, F. A. Dilmanian and D. N. Slatkin, *Nanomedicine (Lond)*, 2013, **8**, 1601-1609.
25. D. Y. Joh, L. Sun, M. Stangl, A. Al Zaki, S. Murty, P. P. Santoiemma, J. J. Davis, B. C. Baumann, M. Alonso-Basanta, D. Bhang, G. D. Kao, A. Tsourkas and J. F. Dorsey, *PLoS One*, 2013, **8**, e62425.
26. L. Bobyk, M. Edouard, P. Deman, M. Vautrin, K. Pernet-Gallay, J. Delaroche, J. F. Adam, F. Esteve, J. L. Ravanat and H. Elleaume, *Nanomedicine*, 2013, **9**, 1089-1097.
27. T. M. Fael Al-Mayhani, S. L. Ball, J. W. Zhao, J. Fawcett, K. Ichimura, P. V. Collins and C. Watts, *J. Neurosci. Methods*, 2009, **176**, 192-199.
28. J. Lee, S. Kotliarova, Y. Kotliarov, A. Li, Q. Su, N. M. Donin, S. Pastorino, B. W. Purow, N. Christopher, W. Zhang, J. K. Park and H. A. Fine, *Cancer Cell*, 2006, **9**, 391-403.
29. K. Kobayashi, N. Usami, E. Porcel, S. Lacombe and C. Le Sech, *Mutat. Res.*, 2010, **704**, 123-131.
30. M. Misawa and J. Takahashi, *Nanomedicine*, 2011, **7**, 604-614.

31. J. Comenge, C. Sotelo, F. Romero, O. Gallego, A. Barnadas, T. G. Parada, F. Dominguez and V. F. Puntes, *PLoS One*, 2012, **7**, e47562.
32. A. Sottoriva, I. Spiteri, S. G. Piccirillo, A. Touloumis, V. P. Collins, J. C. Marioni, C. Curtis, C. Watts and S. Tavare, *Proc. Natl. Acad. Sci. U S A*, 2013, **110**, 4009-4014.
33. L. L. Farrell, J. Pepin, C. Kucharski, X. Lin, Z. Xu and H. Uludag, *Eur. J. Pharm. Biopharm.*, 2007, **65**, 388-397.
34. Y. S. Siu, L. Li, M. F. Leung, K. L. Lee and P. Li, *Biointerphases*, 2012, **7**, 16.
35. Y. Zheng, D. J. Hunting, P. Ayotte and L. Sanche, *Radiat. Res.*, 2008, **169**, 19-27.
36. Y. Q. Peipei Zhang, Chaoming Wang, Liyuan Ma and Ming Su *Nanoscale*, 2014.
37. E. C. Cho, Q. Zhang and Y. Xia, *Nat. Nanotechnol.*, 2011, **6**, 385-391.
38. C. K. Payne, S. A. Jones, C. Chen and X. Zhuang, *Traffic*, 2007, **8**, 389-401.
39. G. Grandinetti, A. E. Smith and T. M. Reineke, *Mol. Pharm.*, 2012, **9**, 523-538.
40. L. Kelland, *Nat. Rev. Cancer*, 2007, **7**, 573-584.
41. D. Wang and S. J. Lippard, *Nat. Rev. Drug Discov.*, 2005, **4**, 307-320.
42. Y. Jung and S. J. Lippard, *Chem. Rev.*, 2007, **107**, 1387-1407.
43. Wang and Z. Guo, *Anticancer Agents Med. Chem.*, 2007, **7**, 19-34.
44. A. R. Timerbaev, C. G. Hartinger, S. S. Aleksenko and B. K. Keppler, *Chem. Rev.*, 2006, **106**, 2224-2248.
45. A. E. Nel, L. Madler, D. Velegol, T. Xia, E. M. Hoek, P. Somasundaran, F. Klaessig, V. Castranova and M. Thompson, *Nat. Mater.*, 2009, **8**, 543-557.
46. J. F. Hainfeld, F. A. Dilmanian, D. N. Slatkin and H. M. Smilowitz, *J. Pharm. Pharmacol.*, 2008, **60**, 977-985.
47. W. Roa, X. Zhang, L. Guo, A. Shaw, X. Hu, Y. Xiong, S. Gulavita, S. Patel, X. Sun, J. Chen, R. Moore and J. Z. Xing, *Nanotechnology*, 2009, **20**, 375101.
48. D. B. Chithrani, S. Jelveh, F. Jalali, M. van Prooijen, C. Allen, R. G. Bristow, R. P. Hill and D. A. Jaffray, *Radiat. Res.*, 2010, **173**, 719-728.
49. B. Jeremic, A. R. Aguerri and N. Filipovic, *Clin. Transl. Oncol.*, 2013, **15**, 593-601.
50. B. D. Chithrani, A. A. Ghazani and W. C. Chan, *Nano Lett.*, 2006, **6**, 662-668.
51. H. S. Choi, W. Liu, P. Misra, E. Tanaka, J. P. Zimmer, B. Itty Ipe, M. G. Bawendi and J. V. Frangioni, *Nat. Biotechnol.*, 2007, **25**, 1165-1170.
52. C. Alric, I. Miladi, D. Kryza, J. Taleb, F. Lux, R. Bazzi, C. Billotey, M. Janier, P. Perriat, S. Roux and O. Tillement, *Nanoscale*, 2013, **5**, 5930-5939.
53. S. Akhter, M. Z. Ahmad, F. J. Ahmad, G. Storm and R. J. Kok, *Expert. Opin. Drug Deliv.*, 2012, **9**, 1225-1243.